

Formation dynamics of an entangled photon pair – a temperature dependent analysis

A. Carmele,* F. Milde, M.-R. Dachner, M. Richter, and A. Knorr
*Institut für Theoretische Physik, Nichtlineare Optik und Quantenelektronik,
Technische Universität Berlin, Hardenbergstraße 36, EW 7-1 10623 Berlin, Germany*

M. Bagheri Harouni and R. Rokniknizadeh
*Physics Department, Quantum Optics Group
University of Isfahan, 81746 Isfahan, Iran*
(Dated: November 4, 2018)

We theoretically study the polarization entanglement of photons generated by the biexciton cascade in a GaAs/InAs semiconductor quantum dot (QD), located in a nano cavity. A detailed analysis of the complex interplay between photon- and carrier coherences and phonons which occurs during the cascade allows us to clearly identify where the entanglement is generated and destroyed. A quantum state tomography is performed for varying exciton fine structure splittings. By constructing an effective multi-phonon Hamiltonian which couples the continuum of the wetting layer states to the QD we investigate the relaxation of the biexciton and exciton states. This consistently introduces a temperature dependence to the cascade. Considering typical Stranski-Karastanov grown QDs, for temperatures around 80 K the degree of entanglement starts to be affected by the dephasing of the exciton states and is ultimately lost above 120 K.

PACS numbers: 78.67.Hc, 42.50.Dv, 63.22.-m, 71.35.-y

I. INTRODUCTION

Coherent superpositions of quantum states allow to outperform the classical bit. Based on this feature the quantum bit (qubit) was introduced.¹ In light of integrated quantum communication, natural candidates for its realization seem to be photonic systems. Not only do their two different polarizations serve as basis states for qubits in quantum computation, but also has encoding and manipulating of quantum information on photons made tremendous advancement: In recent years, photons as qubits have been sent successfully over fiber communication channels,^{2,3} quantum cryptography is already technically feasible^{4,5} and quantum teleportation of so-called entangled photon states was demonstrated.^{6,7} Supported is this development by the convenient fact that linear quantum optics is sufficient, when implementing quantum computing algorithms.⁸

Entanglement in its simplest form is a non-separable superposition of joint quantum states, in our case qubits, that show non-local quantum correlation. Among different proposals^{9,10,11,12,13} very promising solid state source for entangled photon pairs are semiconductor quantum dots (QDs).¹⁴ In contrast to parametric down conversion,¹⁵ where entangled pairs are produced in a probabilistic manner with low efficiency (10^{-10} parametric photons per pump photon¹⁶) radiative decay of a biexciton cascade in QDs provides an on-demand generation of entanglement, a crucial requirement for scalable quantum networks.

The prospect of all-integrated photonic applications in combination with compact semiconductor devices raises the question of how robust and efficient an embedded entangled photon source is when subjected to losses and dephasing due to naturally occurring interaction with its

surrounding host material.

In this respect, Axt *et al.* investigated within a generating functions approach in Ref. 17 the dephasing of an exciton-biexciton-QD system, which is coupled to an arbitrary number of phonon modes and excited by a sequence of δ -shaped classical light pulses, but did not consider the emission of single or entangled photons. With focus on photon entanglement Hohenester *et al.* considered in Ref. 18 the elastic phonon scattering at the device boundaries on a master equation level, assuming an asymmetry in the phonon coupling for different exciton states.

In this paper we present microscopic calculations of a phonon-assisted biexciton cascade in an InAs QD embedded in a InGaAs wetting layer (WL).¹⁹ The coupling of the discrete QD states to the WL continuum via multi-phonon processes²⁰ leads to dephasing rates that significantly limit the entanglement output efficiency for high temperatures (above 100 K).

The coupled dynamics of occupation densities and photon-assisted states in the two-photon emission is treated with an equation of motion (EOM) approach, well-established in solid state optics to approach many-particle problems. This allows us to perform a quantum state tomography and thus calculate the concurrence of the polarization-entangled photons with varying, experimentally controlled external parameters like temperature, exchange splitting, or WL carrier density.

The paper is organized as follows: After the considered system and calculated observables are introduced in more detail in Sec. II, the different interactions of the QD carriers with phonons and cavity photons are discussed in Sec. III. Then the coupled equations of motion are derived, their dynamics solved and the results presented in Sec. III B and IV.

II. CHARACTERIZATION, GENERATION, AND MEASUREMENT OF ENTANGLED PHOTONS

A. Entangled photons and qubits

The two quantum states ($|0\rangle$ and $|1\rangle$) that form a qubit $|Q\rangle$ can encode more information than a classical bit, as a qubit generally exists in a superposition $|Q\rangle = c_1|0\rangle + c_2|1\rangle$ with complex coefficients c_1 and c_2 . In the model regarded here, the physical representation of the qubit states is the superposition of the horizontal $|H\rangle$ and vertical $|V\rangle$ polarization of photons. The true advantage of the quantum approach is reached when two photonic qubits $Q = A, B$ interfere in a non-separable fashion and thus become entangled.¹ The wave function of any entangled qubit $|\psi\rangle_Q$ can be written in the basis of the so-called Bell-states:²¹

$$\begin{aligned} |\Phi^\pm\rangle &= \frac{1}{\sqrt{2}} (|HH\rangle \pm |VV\rangle), \\ |\Psi^\pm\rangle &= \frac{1}{\sqrt{2}} (|HV\rangle \pm |VH\rangle), \end{aligned}$$

where $|HH\rangle = |H_A H_B\rangle = |H\rangle_A |H\rangle_B$, similarly for $|HV\rangle, |VH\rangle, |VV\rangle$. Here, the entangled wave function cannot be expressed as a direct product $|\psi\rangle_Q \neq |\psi_A\rangle_Q \otimes |\psi_B\rangle_Q$ of the wave function of each single qubit. Before going into details of our analysis, we note, that the final photon wave function generated by a biexciton cascade QD emission can be expressed in terms of $|\Phi^\pm\rangle$ only (see discussion below or Ref. 14):

$$\begin{aligned} |\psi\rangle_Q &= \frac{e^{i\theta}}{2} (|\Phi^+\rangle - |\Phi^-\rangle) + \frac{1}{2} (|\Phi^+\rangle + |\Phi^-\rangle) \\ &= \frac{1}{\sqrt{2}} (|HH\rangle + e^{i\theta} |VV\rangle), \end{aligned}$$

where θ is the phase difference between $|HH\rangle$ and $|VV\rangle$. Both systems are in a complete statistical mixture between $|H\rangle$ and $|V\rangle$, but the coherence between $|HH\rangle$ and $|VV\rangle$ is kept. In the HH, HV, VH, VV basis, the two-photon photon density matrix $\rho^{\text{pt}} = |\psi\rangle_Q \langle\psi|$ of the pure $|\psi\rangle_Q$ state can be written as:

$$\rho^{\text{pt}} = |\psi\rangle_Q \langle\psi| = \begin{pmatrix} 1 & 0 & 0 & e^{-i\theta} \\ 0 & 0 & 0 & 0 \\ 0 & 0 & 0 & 0 \\ e^{i\theta} & 0 & 0 & 1 \end{pmatrix}. \quad (1)$$

Following the Peres criterion,²² Eq. (1) indicates entanglement since despite the remaining degree of freedom in θ , the off-diagonal elements representing the coherence between the basis states can never be zero. If, however, these crucial matrix elements $\rho_{VH} = \langle VV | \rho^{\text{pt}} | HH \rangle$ are zero, the system is said to have classical correlation only.

Since we consider entangled photons generated by optical transitions in a biexciton cascade, we introduce the QD's electronic band structure and selection rules in the next subsection.

B. Finestructure of quantum dots and generation of entangled photons

Depending on the intensity, photo-excitation creates in direct gap semiconductors electrons in the WL conduction band and holes in the WL valence band. The carriers subsequently relax into the QD and occupy the discrete energy shells following Pauli's principle.²³ Although relaxed, they still can interact with the WL via multi-phonon processes. To analyze entangled photon emission from a QD, its electronic eigenstates and selection rules for the light-matter interaction have to be known.

Typically, when following a $\mathbf{k} \cdot \mathbf{p}$ approach, the bandstructure of single-InAs QDs around the Γ -point can be approximately described by the two anti-binding s -states of the electrons and the six binding p -states of the holes.²⁴ Due to spin-orbit coupling and strain effects the split-off (SO) and light-hole (LH) states lie energetically well below the heavy-hole (HH) state. Therefore, the relevant single-particle basis is constructed by the heavy-hole with total angular momentum $J_h = 3/2$ and spin projection in growth-direction $m_{j,h} = \pm 3/2$ and the electron with $J_e = 1/2$, $m_{j,e} = \pm 1/2$, all shown in Fig. 1(a). The mutual Coulomb interaction will bind the carriers to electron-hole pairs and so lead to the formation of excitons. Depending on the configurations, given by the projections of the total angular momentum $M = m_{j,e} + m_{j,h}$ four exciton states arise, which can be characterized as optically inactive $M = \pm 2$ (parallel electron and hole spin) and optically active $M = \pm 1$ (anti-parallel spins).²⁵ In a D_{2d} -symmetric QD these bright exciton states, denoted by $|X_\pm\rangle$ are degenerated and couple to σ_\pm circular polarized light [here, σ_+ (σ_-) labels right-hand (left-hand) circular polarized light] as depicted in Fig. 1(b).^{26,27}

The atom-like discrete energy levels of a QD can be pumped electrically or by photo-excitation.²⁸ When the carriers occupy their lowest shell, two excitons can form a bound singlet state, a biexciton ($|B\rangle$). Under emission of the first, σ_+ or σ_- polarized so-called biexciton-photon the system enters into an intermediate, optically allowed exciton state ($|X_\pm\rangle$). Subsequently, the QD relaxes into its ground state ($|G\rangle$) by emitting a second, the exciton-photon. As a consequence of total angular momentum conservation both emitted photons are of opposite circular polarization,²⁹ see Fig. 1(b). Since the exciton states $|X_\pm\rangle$ in symmetric D_{2d} QDs are degenerate (i.e. no fine-structure splitting (FSS) δ is present), the photons' decay path can only be determined by their polarization, otherwise they are indistinguishable. Thus, the cascade will produce a maximally polarization-entangled photon pair wave function $|\psi\rangle_{\text{pt}} = (|HH\rangle + |VV\rangle)/\sqrt{2}$, which corresponds to the $|\Phi^+\rangle$ Bell-state.³⁰

Although growth techniques of single QDs are very sophisticated,³¹ it is rarely possible to not have an asymmetry in the semiconductor crystal and so the non-classical correlation of the photons is often spoiled: Un-

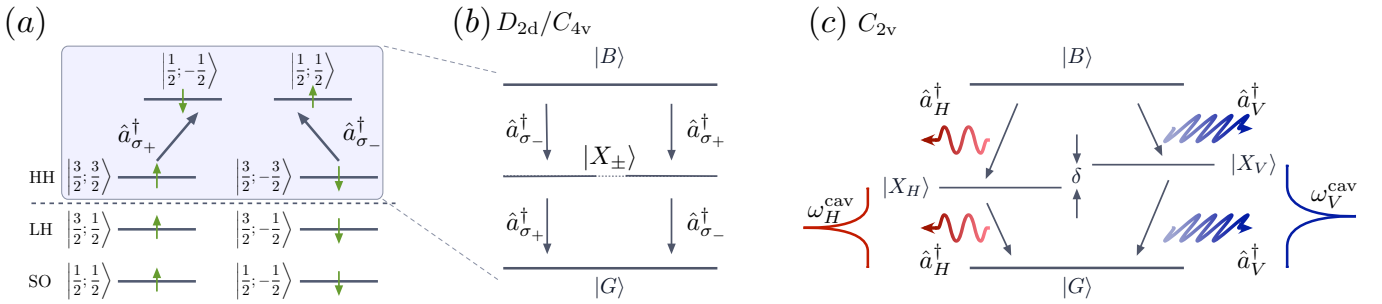


Figure 1: (a) QD band structure with spin states $s = |J; m_j\rangle$. Relevant for the biexcitonic framework are only the electron and heavy hole (HH) states. (b) cascade of a symmetric QD with degenerate exciton states $|X_{\pm}\rangle$. (c) cascade with a FSS $\delta \neq 0$ (without biexcitonic shift). There are two possible paths. Either two photons with vertical V or horizontal H polarization are emitted into a cavity mode $\omega_{V/H}^{\text{cav}}$ with FWHM κ .

For vanishing FSS δ the which-path information is lost and the photons are polarization-entangled. With a FSS $\delta \neq 0$ the photons are not fully polarization-entangled.

der strain the dots symmetry reduces to C_{2v} and the anisotropic electron-hole exchange interaction splits the exciton doublet into two states $|X_H\rangle = 1/\sqrt{2}(|X_+\rangle + |X_-\rangle)$ and $|X_V\rangle = 1/\sqrt{2}(|X_+\rangle - |X_-\rangle)$, energetically separated by the FSS δ , shown in Fig. 1(c). These states couple to photon modes of orthogonal linear polarization along the direction of one crystallographic axis, labeled H and V respectively. This superimposes a which-path information onto the emitted photon frequencies and the degree of their entanglement is reduced. To efficiently collect the photons, the QD is placed inside a cavity supporting only two modes of different polarizations V, H with frequency $\omega_V^{\text{cav}} \neq \omega_H^{\text{cav}}$.³² These modes are assumed to be in resonance with the corresponding exciton-ground state transitions. Although energetically off-resonant, the biexciton-photon is emitted into the same mode, see Fig. 1(c). In principal, the exciton states can be tuned into near resonance again by applying an in-plane external electric^{33,34} or magnetic field,³⁵ and indeed for a small FSS δ generation of polarization-entangled photon pairs was demonstrated on a system operating at 10 K.³⁶

Although the ideal case of zero splitting can be recovered, phonons as a decoherence mechanisms, in particular at elevated temperatures, will have an impact on the performance of a QD as a source of polarization-entangled photons. To provide a meaningful quantitative measure of the entanglement the next section will introduce the concurrence.

C. Measure of entanglement – relevant quantities

As shown in Eq. (1), a measure for the degree of entanglement is determined by the off-diagonal element in the polarization sub-space of the two-photon density matrix ρ^{pt} , explicitly:

$$\rho_{VH} := \langle VV | \rho^{\text{pt}} | HH \rangle. \quad (2)$$

Quantum state tomography³⁷ provides a measurement scheme which gives access to the different elements of

ρ^{pt} . They are experimentally reconstructed by measuring of the two-photon cross correlation function $g_{ij}^2(t, \tau)$ ³⁸ over a mean photon arrival time t . The function $g_{ij}^2(t, \tau)$ corresponds to the polarization correlation between a biexciton-photon emitted at time t and the subsequent exciton-photon at time $t + \tau$.³⁹

$$g_{ij}^2(t, \tau) \propto \langle a_i^{\dagger}(t) a_i^{\dagger}(t + \tau) a_j(t + \tau) a_j(t) \rangle, \quad (3)$$

where $i, j \in \{H, V\}$. The correlation function is written in terms of photon creation a_i^{\dagger} and annihilation a_j operators of the different photon modes i, j , cp. Fig. 1(c). We consider an experimental setup, where the time delay between the two photons τ is zero. This can be realized by appropriately adjusting the distance to the detector.^{36,40} The temporal dynamics of the corresponding density matrix element $\langle ii | \rho^{\text{pt}} | jj \rangle$ is obtained when the second-order correlation function $g_{ij}^2(t, \tau = 0)$ is time averaged over the arrival times t :³⁹

$$\langle ii | \rho^{\text{pt}} | jj \rangle(t) = \frac{1}{t} \int_0^t g_{ij}^2(t', 0) dt'. \quad (4)$$

Thus, the source of entanglement can be rewritten as $\rho_{HV} \propto \langle \hat{a}_V^{\dagger} \hat{a}_V^{\dagger} \hat{a}_H \hat{a}_H \rangle$. A standard expression for the degree of entanglement is the concurrence C :^{41,42}

$$C = 2|\rho_{HV}|, \quad (5)$$

directly related to other accepted measures like the entanglement of formation⁴³ E_F or the tangle⁴⁴ T (for example, $C = \sqrt{T}$). Here, $C = 1$ corresponds to maximum entanglement and $C = 0$ to zero entanglement. To calculate the necessary dynamics of the expectation values, e.g. $\langle \hat{a}_V^{\dagger} \hat{a}_V^{\dagger} \hat{a}_H \hat{a}_H \rangle$, a set of equations is derived in the next section.

III. MODELING AN EMBEDDED QUANTUM DOT AS A SEMICONDUCTOR SOURCE OF ENTANGLEMENT

A. Hamiltonian and QD model

The coupled dynamics of observables, such as Eq. (3) can be generally derived from the system's Hamilton operator \hat{H} via Heisenberg's equation of motion:

$$-i\hbar\partial_t \langle \hat{O} \rangle = \langle [\hat{H}, \hat{O}]_- \rangle. \quad (6)$$

In this section, we discuss the used Hamiltonian to implement our model system. Applying Eq. (6) to the photon correlation function g_{ij}^2 introduces a coupling to the electronic degrees of freedom via the electron-photon interaction. As discussed in Sec. II B, due to strong confinement, we assume that the QD single-particle states are energetically well separated and only the highest valance (v) HH state and lowest conduction (c) band s -shell form the biexcitonic framework, see again Fig. 1. In second quantization Fermionic operators describe the typical electron-hole representation, where carriers are the heavy holes in the v band (operator \hat{h}_s) and electrons in the c band (denoted by operator \hat{e}_s). Here, the carrier spin state $s = |J, m_j\rangle$ is given for the holes (electrons) by $\uparrow = |3/2; 3/2\rangle$ ($\uparrow = |1/2; 1/2\rangle$) and $\downarrow = |3/2; -3/2\rangle$ ($\downarrow = |1/2; -1/2\rangle$).

The complete Hamiltonian of a QD coupled to the WL continuum inside a nanocavity consists of various parts and is given as:

$$\begin{aligned} \hat{H} = & \hat{H}_{\text{QD},0}^c + \hat{H}_{\text{QD}}^{c-c} + \hat{H}_0^{\text{pt}} + \hat{H}_{\text{QD}}^{c-\text{pt}} \\ & + \hat{H}_{\text{WL},0}^c + \hat{H}_0^{\text{pn}} + \hat{H}_{\text{QD,WL}}^{c-\text{pn}} + \hat{H}_{\text{WL,WL}}^{c-\text{pn}}. \end{aligned} \quad (7)$$

First, the kinetic energy of the confined QD carriers $\hat{H}_{\text{QD},0}^c$ and their mutual carrier-carrier interaction $\hat{H}_{\text{QD}}^{c-c}$ are introduced. The electron-hole pair in the QD does interact with the cavity photons of the quantized light field $\hat{H}_{\text{QD}}^{c-\text{pt}}$ and so the free energy of the cavity photons \hat{H}_0^{pt} is included as well. The free energy of semiconductor bulk phonons \hat{H}_0^{pn} and WL carriers $\hat{H}_{\text{WL},0}^c$ appears, too. The interaction of the WL with the QD states via LO-phonons is considered in $\hat{H}_{\text{QD,WL}}^{c-\text{pn}}$ and the electron-phonon coupling within the WL in $\hat{H}_{\text{WL,WL}}^{c-\text{pn}}$. The contributions to the \hat{H}_0 part read:

$$\begin{aligned} \hat{H}_{\text{QD},0}^c &= \sum_s \varepsilon_v^{\text{QD}} \hat{h}_s^\dagger \hat{h}_s + \varepsilon_c^{\text{QD}} \hat{e}_s^\dagger \hat{e}_s, \\ \hat{H}_0^{\text{pn}} &= \sum_{\mathbf{q}} \hbar\omega_{\text{LO}} \hat{b}_{\mathbf{q}}^\dagger \hat{b}_{\mathbf{q}}, \\ \hat{H}_{\text{WL},0}^c &= \sum_{\mathbf{k}s} \varepsilon_{v\mathbf{k}}^{\text{WL}} \hat{w}_{\mathbf{k}s}^\dagger \hat{w}_{\mathbf{k}s}, \\ \hat{H}_0^{\text{pt}} &= \sum_i \hbar\omega_i \hat{a}_i^\dagger \hat{a}_i. \end{aligned}$$

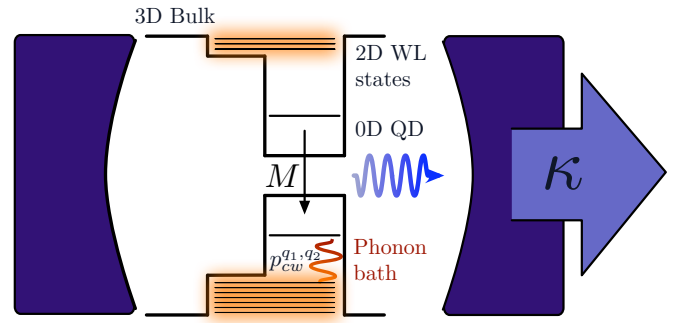


Figure 2: General system scheme. Two electron-hole pairs in a QD are coupled to the continuum of WL states via LO-phonon interaction $p_{cw}^{q1, q2}$. The phonons are in a thermal bath. The QD has two levels with a conduction and a valence band. Here, the carriers interact with photons via the electron-light coupling elements M . The QD is assumed to be placed at a node position of the electromagnetic field in a cavity. Since its loss $\kappa = 10 \mu\text{eV}$ is greater than the coupling strength to the field $M = 1 \mu\text{eV}$, the system is in a weak coupling regime.

The Bosonic longitudinal optical (LO) phonon creation (annihilation) operators at wave vector \mathbf{q} are $\hat{b}_{\mathbf{q}}^\dagger$ ($\hat{b}_{\mathbf{q}}$). Their dispersion is treated within the Einstein approximation and $\hbar\omega_{\text{LO}} = 36 \text{ meV}$. Similar to the QD operators $\hat{w}_{\mathbf{k}s}^\dagger$ ($\hat{w}_{\mathbf{k}s}$) are creators (annihilators) of a hole carrier in the WL continuum of the valence band v with spin state s and wave vector \mathbf{k} . For the WL carriers, we take into account only the hole contributions of the v band, motivated in the next section. The impact of spin-orbit coupling on the carrier's energy can be neglected in QDs⁴⁵ and so, ε_i is assumed to be independent of the carrier's spin state. The general considered setup is displayed in Fig. 2. The next subsections discuss the remaining parts of the total Hamiltonian separately and in more detail. The electron-phonon interaction Hamiltonian leads to temperature dependent dephasing rates (see subsection III A 1). The pure electronic part of non-interacting and Coulomb-interacting QD electrons $\hat{H}_{\text{QD},0}^c + \hat{H}_{\text{QD}}^{c-c}$ is diagonalized and transformed into an excitonic basis. The new arising eigenvalues and eigenvectors will incorporate the complete Coulomb contributions (see subsection III A 2), which are energy shifts (e.g. ground state and biexciton shift) and the exchange splitting due to different spin combinations in the exciton states. In the excitonic basis, the electron-photon interaction is transformed and new orthogonal field modes are derived (see subsection III A 3).

1. Multi-phonon coupling of WL and QD

Embedded in a host material, quantum confined electrons in Stranski-Krastanov grown InAs/GaAs QDs interact via LO-phonons with a continuum of two dimensional electronic WL states only a few ten meV away.

This leads to temperature dependent dephasing times for the QD states^{46,47,48,49} and can be a first approach to the problem of temperature dependent generation of entangled photon pairs. On the time scale of several nanoseconds regarded here, longitudinal acoustical phonons^{50,51} only have a minor impact and are not considered.

Depending on the dot size,²³ the QD valence band is typically more than one, but less than two LO-phonon energies $\hbar\omega_{\text{LO}}$ energetically separated from the WL band edge, see Fig. 3. To effectively connect the QD states with the WL, up to two-phonon processes have to be taken into account. Within the two-phonon limit the influence of the WL conduction band on the QD electrons can be neglected, because here, more than two LO-phonons are necessary to bridge the energy gap to the WL and therefore the dephasing is determined by the hole-WL interaction. Moreover, the Coulomb interaction of the WL carriers is not included as the carrier densities considered here are low.⁵² Under these assumptions, microscopic dephasing rates are derived by using an effective Hamiltonian approach, which originates from a multi-photon theory.⁵³ From the Hamiltonian in Eq. (7) the following parts contribute to the LO-phonon induced dephasing:

$$\begin{aligned} \hat{H}_{\text{QD,WL}} = & \hat{H}_{\text{QD},0}^{\text{c}} + \hat{H}_{\text{WL},0}^{\text{c}} \\ & + \hat{H}_0^{\text{pn}} + \hat{H}_{\text{QD,WL}}^{\text{c-pn}} + \hat{H}_{\text{WL,WL}}^{\text{c-pn}}. \end{aligned} \quad (8)$$

The phonon mediated interaction between QD holes and WL states and the carrier-phonon interaction within the WL are given by

$$\begin{aligned} \hat{H}_{\text{QD,WL}}^{\text{c-pn}} = & \sum_s \sum_{\mathbf{k}\mathbf{q}} g_{0\mathbf{k}}^{\mathbf{q}} \hat{h}_s^\dagger \hat{w}_{\mathbf{k}s} (\hat{b}_{\mathbf{q}} + \hat{b}_{-\mathbf{q}}^\dagger) + \text{h.a.}, \\ \hat{H}_{\text{WL,WL}}^{\text{c-pn}} = & \sum_s \sum_{\mathbf{k}\mathbf{k}'\mathbf{q}} g_{\mathbf{k}\mathbf{k}'}^{\mathbf{q}} \hat{w}_{\mathbf{k}s}^\dagger \hat{w}_{\mathbf{k}'s} (\hat{b}_{\mathbf{q}} + \hat{b}_{-\mathbf{q}}^\dagger) + \text{h.a.} \end{aligned}$$

The Fröhlich coupling elements are $g_{\mathbf{k}\mathbf{k}'}^{\mathbf{q}}$ which can be found in Ref. 54. Within a projection operator based theory⁵³ Eq. (8) is mapped onto the resonant WL states only and becomes:

$$\hat{H}_{\text{QD,WL}} = \hat{H}_{\text{QD},0}^{\text{c}} + \hat{H}_{\text{WL},0}^{\text{c}} + \hat{H}_{\text{eff}}, \quad (9)$$

with the effective LO-phonon-assisted WL influence on the QD holes in \hat{H}_{eff} . All other off-resonant contributions are implicitly included in the coupling elements of the effective Hamiltonian. Taking only two-phonon processes into account, \hat{H}_{eff} reads:⁵⁵

$$\begin{aligned} \hat{H}_{\text{eff}} = & \sum_s \sum_{\mathbf{q}_1 \mathbf{q}_2 \mathbf{k}_{\text{res}}} p_{c_w,s}^{\mathbf{q}_1 \mathbf{q}_2} \hat{h}_s^\dagger \hat{w}_{\mathbf{k}_{\text{res}}s} \hat{b}_{\mathbf{q}_1} \hat{b}_{\mathbf{q}_2} \\ & + \sum_s \sum_{\mathbf{q}_1 \mathbf{q}_2 \mathbf{k}_{\text{res}}} p_{w_c,s}^{\mathbf{q}_1 \mathbf{q}_2} \hat{w}_{\mathbf{k}_{\text{res}}s}^\dagger \hat{h}_s \hat{b}_{\mathbf{q}_1}^\dagger \hat{b}_{\mathbf{q}_2}^\dagger, \end{aligned}$$

with the effective coupling elements

$$p_{c_w,s}^{\mathbf{q}_1 \mathbf{q}_2} = \sum_{\substack{\mathbf{k} \\ \mathbf{k} \neq \mathbf{k}_{\text{res}}}} \frac{g_{0\mathbf{k}}^{\mathbf{q}_1} g_{\mathbf{k}\mathbf{k}_{\text{res}}}^{\mathbf{q}_2} (1 - \langle \hat{w}_{\mathbf{k}s}^\dagger \hat{w}_{\mathbf{k}s} \rangle)}{\varepsilon_{v\mathbf{k}}^{\text{WL}} - \varepsilon_v^{\text{QD}} - \hbar\omega_{\text{LO}}}. \quad (10)$$

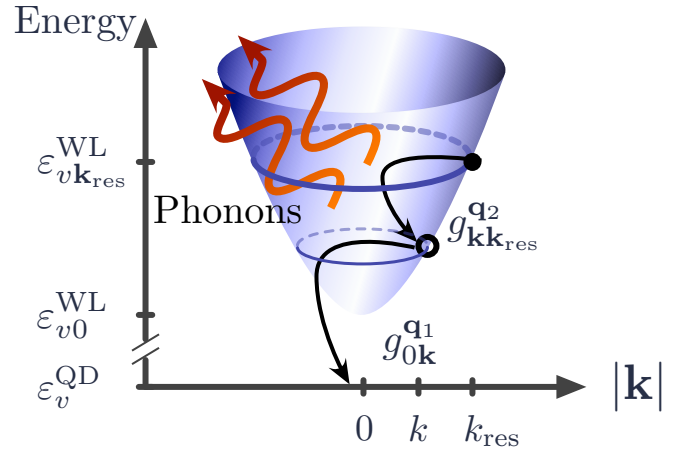


Figure 3: Wetting layer system scheme. Seen in blue is the 2D dispersion of the WL holes $\hbar^2\mathbf{k}^2/(2m_h^*)$. Marked on the energy scale are (i) the WL band edge $\varepsilon_{v0}^{\text{WL}}$ which is energetically separated from the QD v shell $\varepsilon_v^{\text{QD}}$ by more than a single-phonon energy: $\Delta\varepsilon_v^{\text{QD}} = \varepsilon_{v0}^{\text{WL}} - \varepsilon_v^{\text{QD}} > \hbar\omega_{\text{LO}}$, (ii) the WL states at \mathbf{k}_{res} resonant with a two-phonon transition $\varepsilon_{v\mathbf{k}_{\text{res}}}^{\text{WL}} = \varepsilon_v^{\text{QD}} + 2\hbar\omega_{\text{LO}}$ to the QD.

The transition from the resonant states to the QD pass through intermediate states at $\varepsilon_{v\mathbf{k}}^{\text{WL}}$ with probability amplitude $g_{\mathbf{k}\mathbf{k}_1}^{\mathbf{q}_1}$.

They contain Pauli blocking terms and therefore depend on temperature and WL carrier occupation $(1 - \langle \hat{w}_{\mathbf{k}s}^\dagger \hat{w}_{\mathbf{k}s} \rangle)$.⁵⁶ The WL holes in \hat{H}_{eff} have an energy exactly two phonon energies away from the QD state energy. A transition from these resonant WL holes at $\varepsilon_{v\mathbf{k}_{\text{res}}}^{\text{WL}}$ to the QD shell takes place under simultaneous emission of two phonons. The whole process is energy conserving: $\varepsilon_{v\mathbf{k}_{\text{res}}}^{\text{WL}} - \varepsilon_v^{\text{QD}} = 2\hbar\omega_{\text{LO}}$. Within time-energy uncertainty carriers relax by a higher-order Markov process. Here, in the transition to the intermediate state at $\varepsilon_{v\mathbf{k}}^{\text{WL}}$ energy conservation is violated, since the hole state at \mathbf{k} is less than $\hbar\omega_{\text{LO}}$ from $\varepsilon_{v\mathbf{k}_{\text{res}}}^{\text{WL}}$ and more than $\hbar\omega_{\text{LO}}$ from the QD state energetically separated, see Fig. 3. The probability amplitude for the intermediate transitions are $g_{\mathbf{k}\mathbf{k}_{\text{res}}}^{\mathbf{q}_2}$ and $g_{0\mathbf{k}}^{\mathbf{q}_1}$. Equation (10) shows that all possible transitions between QD and WL are mediated by all off-resonant WL states \mathbf{k} . The strength of the coupling element is determined by to what extent the energy conservation condition in the denominator is met in every phonon-assisted electronic transition. We can use the effective Hamiltonian Eq. (9) to derive relaxation and dephasing rates using Heisenberg equations of motion, where the hierarchy problem is treated within a born factorization.⁵⁷ The calculations lead to the following equations for the QD states:

$$\frac{d}{dt} \langle \hat{e}_s^\dagger \hat{h}_s^\dagger \rangle = -(i\hbar\Omega_0 + \Gamma_{w,s}) \langle \hat{e}_s^\dagger \hat{h}_s^\dagger \rangle, \quad (11)$$

$$\frac{d}{dt} \langle \hat{h}_s^\dagger \hat{h}_s \rangle = -2\Gamma_{w,s} \langle \hat{h}_s^\dagger \hat{h}_s \rangle, \quad (12)$$

with the QD gap energy $\hbar\Omega_0 = \varepsilon_c^{\text{QD}} - \varepsilon_v^{\text{QD}}$ and the WL-

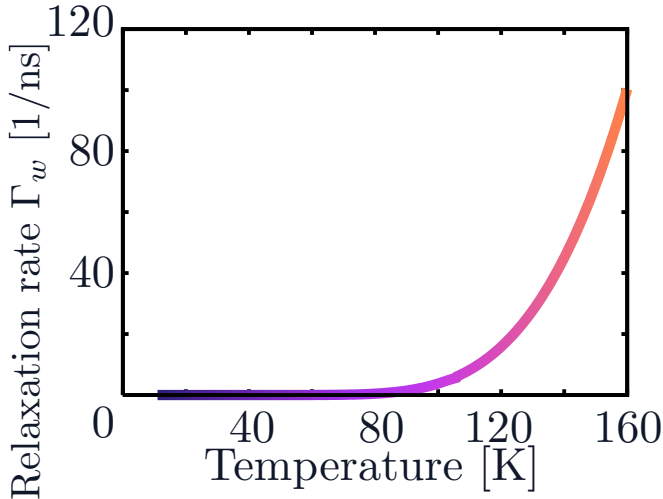


Figure 4: Plot of the phonon-induced relaxation rate Γ_w as a function of temperature T . At about 80 K Γ_w has approached 1 ns^{-1} and starts to contribute strongly to the decay of the QD states.

induced damping rate:⁵⁵

$$\Gamma_{w,s} = [(1 - f_{h,s})(n + 1)^2 + f_{h,s}n^2] \gamma_s. \quad (13)$$

The damping γ_s is given by:

$$\gamma_s = \iint d^3q_1 d^3q_2 \quad p_{cw,s}^{\mathbf{q}_1\mathbf{q}_2} (p_{wc,s}^{\mathbf{q}_1\mathbf{q}_2} + p_{wc,s}^{\mathbf{q}_2\mathbf{q}_1}). \quad (14)$$

In Eq. (13) $f_{h,s} = \sum_{\mathbf{k}_{\text{res}}} \langle \hat{w}_{\mathbf{k}_{\text{res}}s}^\dagger \hat{w}_{\mathbf{k}_{\text{res}}s} \rangle$ is used for the WL hole density at the resonant energy, which in the carrier low-density limit is assumed to be zero. Note, that this implies $\Gamma_w = \Gamma_{w,\uparrow} = \Gamma_{w,\downarrow}$. Since the system has relaxed into a quasi-equilibrium, the phonon bath is described by the Bose-Einstein distribution $n = \langle \hat{b}^\dagger \hat{b} \rangle$. Figure 4 displays the temperature dependence of Γ_w . In the next section an excitonic basis will be introduced. The damping rates in Eqs. (11) and (12) will be used in this basis to account for the relaxation of the QD electrons.⁵⁸

2. Carrier-carrier interaction and exciton representation

The Hamiltonian in Eq. (7) accounting for the QD carriers and their interaction via the Coulomb potential $\hat{H}_{\text{Coul}} = \hat{H}_{\text{QD},0}^{\text{c}} + \hat{H}_{\text{QD}}^{\text{c-c}}$ is conveniently rewritten as:¹⁷

$$\begin{aligned} \hat{H}_{\text{Coul}} = & \sum_s \frac{\hbar\Omega_0}{2} \left(\hat{e}_s^\dagger \hat{e}_s - \hat{h}_s^\dagger \hat{h}_s \right) \\ & + \frac{1}{2} \sum_{ss'} \left(V^{ee} \hat{e}_s^\dagger \hat{e}_s \hat{e}_{s'}^\dagger \hat{e}_{s'} + V^{hh} \hat{h}_s^\dagger \hat{h}_s \hat{h}_{s'}^\dagger \hat{h}_{s'} \right. \\ & \left. + 2V_{ss'}^{\text{ex}} \hat{e}_s^\dagger \hat{e}_s \hat{h}_{s'}^\dagger \hat{h}_{s'} - 2V^{he} \hat{e}_s^\dagger \hat{e}_s \hat{h}_{s'}^\dagger \hat{h}_{s'} \right). \end{aligned} \quad (15)$$

Table I: Numerical parameters.

Parameter	Symbol	Value
electron effective mass	m_e	$0.043m_0$ ⁶⁴
hole effective mass	m_h	$0.450m_0$ ⁶⁴
LO-phonon energy	$\hbar\omega_{\text{LO}}$	36.4 meV ⁶⁴
QD band gap	$\hbar\omega_0$	1.5 eV
hole binding energy	$\Delta\epsilon_v$	$1.5 \hbar\omega_{\text{LO}}$
Coulomb parameters	$V^{vc} = V^{vv} = V^{cc}$	$25 \mu\text{eV}$
	$V_{\uparrow\uparrow}^{\text{ex}} = V_{\downarrow\downarrow}^{\text{ex}}$	$0 \mu\text{eV}$
photon lifetime in a cavity	κ	$10 \mu\text{eV}$
electron-photon coupling	M	$1 \mu\text{eV}$
photon lifetime	Γ_{rad}	50 ps^{-1}

The first term contains the non-interacting electrons with gap energy $\hbar\Omega_0$. The second term accounts for the repulsion of carriers within the same band, whereas the last term gives attractive direct Coulomb interaction and repulsive exchange interaction between carriers in different bands. The corresponding Coulomb elements $V^{ee}, V^{hh}, V^{he}, V_{ss'}^{\text{ex}}$ mediate the interaction. Responsible for the fine structure splitting δ , compare Fig. 1, is the exchange splitting $V_{\uparrow\downarrow}^{\text{ex}}$, which describes the repulsion and attraction forces induced by different spin-conformations of electrons and holes. As shown in App. A the FSS can be expressed by

$$\delta = 2 |V_{\uparrow\downarrow}^{\text{ex}}|. \quad (16)$$

To simplify the notation we will refer to $V_{\uparrow\downarrow}^{\text{ex}}$ as V_{ex} .

In principle, all matrix elements of the Coulomb interaction can be microscopically calculated, when the single-particle wave functions are known.^{59,60,61,62} However, their values only have a quantitative impact on the results. Therefore, within a reasonable range, they are used as model parameters, measured in experiments.⁶³ Using the space spanned by the new exciton operators, derived in App. A, the Hamiltonian is rewritten as:⁶¹

$$\begin{aligned} \hat{H}_{\text{Coul}} = & \hbar\omega_G \hat{G}^\dagger \hat{G} + \hbar\omega_H \hat{X}_H^\dagger \hat{X}_H \\ & + \hbar\omega_V \hat{X}_V^\dagger \hat{X}_V + \hbar\omega_B \hat{B}^\dagger \hat{B}, \end{aligned}$$

with \hat{G} the ground state, $\hat{X}_{H/V}$ the exciton and \hat{B} the biexciton annihilation operator, corresponding to the excitonic level structure as depicted in Fig. 1(c). Note, that within this diagonal representation the derivation of equations of motion via Eq. (6) is trivial for the Coulomb interaction, as operators of different states commute.

3. QD electron-photon interaction

Commonly, the Hamiltonian of the electron-photon interaction is taken in rotating-wave approximation:³⁸

$$\hat{H}_{\text{QD}}^{\text{c-pt}} = \hbar M \sum_i \left(\hat{h}_\uparrow \hat{e}_\downarrow \hat{a}_{i\sigma_+}^\dagger + \hat{h}_\downarrow \hat{e}_\uparrow \hat{a}_{i\sigma_-}^\dagger \right) + \text{h.a.}, \quad (17)$$

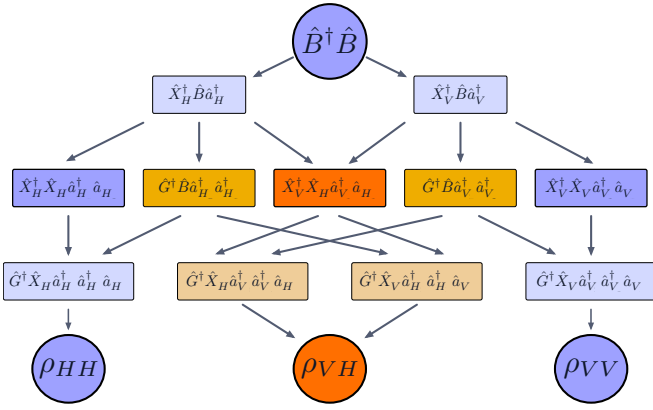


Figure 5: Equations of motion, truncated to the pure cascade scheme. The dark blue quantities represent densities which do not contribute to entanglement, whereas the dark orange and red quantities directly generate a crossing of the different paths in the light orange boxes and are crucial to entanglement.

where the corresponding spin states couple to circular σ_{\pm} polarized light (see Sec. II B for more detail), i is the mode of the emitted photon and M denotes the electron-photon coupling matrix elements. The Hamiltonian of the light-electron interaction is expressed with the exciton operators, derived in the App. B:

$$\hat{H}_{\text{QD}}^{\text{c-pt}} = \hbar M \sum_i \left(\hat{G}^\dagger \hat{X}_H \hat{a}_{iH}^\dagger + \hat{G}^\dagger \hat{X}_V \hat{a}_{iV}^\dagger \right) \quad (18)$$

$$+ \hbar M \sum_i \left(\hat{X}_H^\dagger \hat{B} \hat{a}_{iH}^\dagger - \hat{X}_V^\dagger \hat{B} \hat{a}_{iV}^\dagger \right) + \text{h.a.}$$

We assume that our QD is placed at a node position inside a nano-cavity, which provides two different modes for the different polarizations H and V corresponding to different frequencies $\omega_H \neq \omega_V$.³² Since only two modes exist within the cavity we investigate a cavity-enhanced biexciton cascade. However, we remain in the weak coupling regime since the cavity loss $\kappa = 10 \mu\text{eV}$ is greater than the coupling strength to the field $M = 1 \mu\text{eV}$. Regarding only these two modes, the electron-light interaction Hamiltonian can be written in a compact form

$$\hat{H}_{\text{QD}}^{\text{c-pt}} = \hbar M \left(\hat{G}^\dagger \hat{X}_H \hat{a}_H^\dagger + \hat{G}^\dagger \hat{X}_V \hat{a}_V^\dagger \right. \\ \left. + \hat{X}_H^\dagger \hat{B} \hat{a}_H^\dagger - \hat{X}_V^\dagger \hat{B} \hat{a}_V^\dagger \right) + \text{h.a.} \quad (19)$$

At this status, the total Hamiltonian is written with the new exciton and photon operators (H, V). To discuss the polarization entanglement between two emitted photons we proceed and determine equations of motion, which govern the relevant observables' dynamics.

B. Equations of motion

To derive the coupled dynamics of photon-polarization coherences and electronic transitions with Heisenberg's

equation of motion Eq. (6),^{65,66} the total excitonic Hamiltonian

$$\hat{H} = \sum_{i=H,V} \hbar \omega_i^{\text{cav}} \hat{a}_i^\dagger \hat{a}_i + \hbar \omega_G \hat{G}^\dagger \hat{G} + \hbar \omega_H \hat{X}_H^\dagger \hat{X}_H \\ + \hbar \omega_V \hat{X}_V^\dagger \hat{X}_V + \hbar \omega_B \hat{B}^\dagger \hat{B} + \hbar M \left(\hat{G}^\dagger \hat{X}_H \hat{a}_H^\dagger \right. \\ \left. + \hat{G}^\dagger \hat{X}_V \hat{a}_V^\dagger + \hat{X}_H^\dagger \hat{B} \hat{a}_H^\dagger - \hat{X}_V^\dagger \hat{B} \hat{a}_V^\dagger + \text{h.a.} \right)$$

in conjunction with the temperature dependent relaxation rates Γ_w given in Eq. (13) is used. The latter lead to an additional decay of the QD populations and dephasing contributions to the QD transitions. Those contributions are derived via the effective Hamiltonian approach in Sec. III A 1 and are consistently included by higher-order Markov approximations of the phonon-mediated interaction between carriers in the WL and QD.⁵⁸

An overview of the, at a first glance complicated coupled dynamics of the considered correlation functions (derived by Eq. 6), is given in Fig. 5. Going through the scheme, step by step we unravel the consequential interplay of the different quantities. An initially given biexciton density can decay via two possible paths (left H , right V) and generate a photon pair ρ_{ij} ($i, j \in \{H, V\}$). In a first step, a photon-assisted coherence builds up $\hat{X}_i^\dagger \hat{B} \hat{a}_i^\dagger$ (light blue box), which then contributes to (i) a cross-polarization coherence $\hat{X}_V^\dagger \hat{X}_H \hat{a}_V^\dagger \hat{a}_H$ (red box) particularly important to achieve entanglement in ρ_{VH} . (ii) a two-photon coherence $\hat{G}^\dagger \hat{B} \hat{a}_i^\dagger \hat{a}_i^\dagger$ (light orange box), which also leads to an interference of the two path and thus contributes to ρ_{VH} . (iii) a combined exciton-photon density $\hat{X}_i^\dagger \hat{X}_i \hat{a}_i^\dagger \hat{a}_i$ (dark blue box), which does not influence the degree of entanglement. This gives meaningful insights to the underlying physics and origin of polarization entanglement. Note, that we are in a weak coupling regime and only spontaneous emission in the cascade is taken into account.

The concurrence C as a measure for the degree of entanglement is determined by the photon density matrix, cf. Eq. (5), and defined via the off-diagonal element ρ_{VH} :

$$\partial_t \langle \hat{a}_V^\dagger \hat{a}_V^\dagger \hat{a}_H \hat{a}_H \rangle = \quad (20)$$

$$2i (\omega_V^{\text{cav}} - \omega_H^{\text{cav}} + 2i\kappa) \langle \hat{a}_V^\dagger \hat{a}_V^\dagger \hat{a}_H \hat{a}_H \rangle \\ + 2iM \left(\langle \hat{G}^\dagger \hat{X}_H \hat{a}_V^\dagger \hat{a}_V^\dagger \hat{a}_H \rangle - \langle \hat{X}_V^\dagger \hat{G} \hat{a}_V^\dagger \hat{a}_H \hat{a}_H \rangle \right).$$

Beside its damping due to cavity losses⁶⁷ chosen to be $\kappa = 10 \mu\text{eV}$, the two-photon correlation ρ_{VH} is driven by two higher-order quantities. Both include an exciton-ground state transition under emission of a photon of opposite polarization as the $|X_i\rangle$ state would allow, e.g. $\hat{G}^\dagger \hat{X}_H \hat{a}_V^\dagger$ (the complex conjugate of $\hat{G}^\dagger \hat{X}_V \hat{a}_H$). The transition process takes place under presence of a photon coherence $\hat{a}_V^\dagger \hat{a}_H$ generated by the previous biexciton-exciton decay, see light-orange boxes in Fig. 5. As these terms already include a single-photon coherence and generate a second one leading to a two-photon coherence,

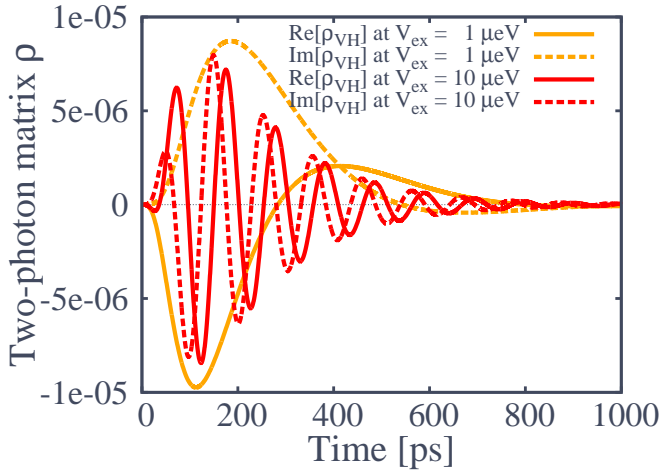


Figure 6: Temporal evolution of the non-integrated off-diagonal two-photon density matrix elements at $T = 0$ K (real (solid) and imaginary (dashed) part) for $V_{\text{ex}} = 1 \mu\text{eV}$ (orange) and $V_{\text{ex}} = 10 \mu\text{eV}$ (red). With increasing V_{ex} the oscillations become more rapid.

they are exactly the terms one would expect to contribute to ρ_{VH} . For a small FSS, the fixed cavity frequencies ω_V^{cav} and ω_H^{cav} are in near-resonance and ρ_{VH} will slowly oscillate on the timescale given by the corresponding FSS, see the orange curves (all at $T = 0$ K) in Fig. 6. For an increasing FSS on the other hand both frequencies are detuned and ρ_{VH} shows a strong oscillating behavior, compare red curves in Fig. 6. Here, the temporal mean value of ρ_{VH} is close to zero and thus no entanglement in a measurement is observed, compare with red curve (all at $T = 0$ K) in Fig. 7 for the integrated ρ_{VH} . In a physical interpretation that means the two different decay paths are distinguishable, so either the photons are entirely emitted in the H or V cascade, but there is no overlap which is only generated by transitions like $\hat{G}^\dagger \hat{X}_H \hat{a}_V^\dagger$, containing both V, H indices. The which-path information is conserved. If there is an uncertainty in the decay path, the photons become partially polarization-entangled.

The quantities in this section are damped by the LO-phonon-assisted WL influence as motivated in section III A 1. The calculated damping rates Γ_w from Eqs. (11) and (12) correspond to a T_1 -time and are incorporated like the radiative dephasing Γ_{rad} in the Weisskopf-Wigner theory.^{62,68} Both occur and lead to an overall damping of $\Gamma = \Gamma_{\text{rad}} + \Gamma_w$:

$$\begin{aligned} \partial_t \langle \hat{B}^\dagger \hat{B} \rangle &\propto -4\Gamma \langle \hat{B}^\dagger \hat{B} \rangle, \\ \partial_t \langle \hat{X}_i^\dagger \hat{B} \hat{a}_i \rangle &\propto -3\Gamma \langle \hat{X}_i^\dagger \hat{B} \hat{a}_i \rangle, \\ \partial_t \langle \hat{X}_i^\dagger \hat{X}_i \hat{a}_i^\dagger \hat{a}_i \rangle &\propto -2\Gamma \langle \hat{X}_i^\dagger \hat{X}_i \hat{a}_i^\dagger \hat{a}_i \rangle, \\ \partial_t \langle \hat{G}^\dagger \hat{X}_i \hat{a}_i \rangle &\propto -1\Gamma \langle \hat{G}^\dagger \hat{X}_i \hat{a}_i \rangle. \end{aligned}$$

The exciton \hat{X}_i is damped by the mere presence of the

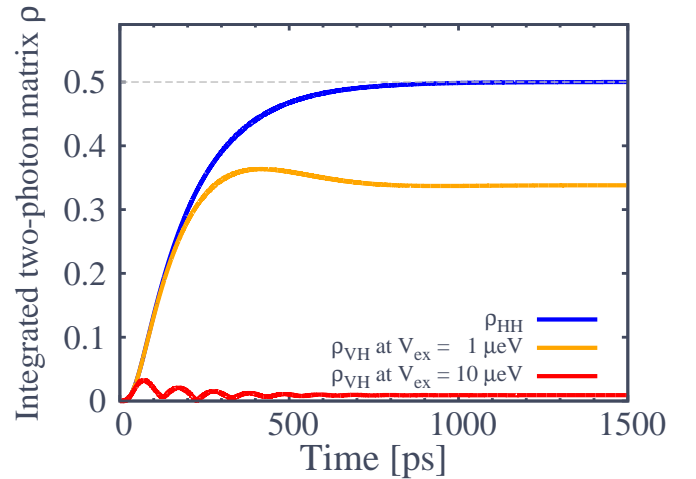


Figure 7: Integrated two-photon matrix elements at $T = 0$ K. Their steady-state values give the quantum state tomography.

empty WL states as they disturb the system and lead to a decoherence. This introduces a temperature dependence to the cascade, which is inherited to the perturbation induced by the coupling to the WL and thus included in $\Gamma_w = \Gamma_w(T)$ motivated in Sec. III A 1.

By numerically solving the set of Eqs. (20, C1-C14) given in App. C we will investigate how the temperature affects the concurrence. Later, the complete temporal dynamics of the cascade presented already partially in this section is resolved.

IV. RESULTS - DYNAMICS OF THE BIEXCITON CASCADE AND QUALITY OF ENTANGLEMENT

Since ρ^{pt} is experimentally reconstructed by photo-counting experiments all elements of ρ^{pt} are given by time-averaging.³⁹ Recalling and employing Eq. (3) to the results of Fig. 6, where already the temporal evolution of ρ^{pt} elements is given we get its integrated elements. As can be seen in Fig. 7 the diagonal elements have a continuous positive slope and start to saturate around 0.5 ns. The steady state which determines the quantum state tomography is reached at 1 ns. However, the situation is very different for the off-diagonal elements, as they are complex quantities that oscillate when $V_{\text{ex}} \neq 0$. Its absolute value (important for the concurrence) shows a non-monotonous behavior in Fig. 7. Obviously, the concurrence is lost for a FSS higher than $V_{\text{ex}} = 10 \mu\text{eV}$.

Since all steady-state elements of ρ^{pt} are given by time-averaging, C will drop for increasing V_{ex} as the integrated ρ_{VH} did. This can be clearly seen in the quantum state tomography shown in Fig. 8. The diagonal and off-diagonal contributions are still in the same order of magnitude for $V_{\text{ex}} = 1 \mu\text{eV}$ cp. Fig. 8(a), but a loss can already be seen. For a larger splitting ρ_{VH} vanishes in Fig. 8(b). Figure 9 constitutes the central result of this

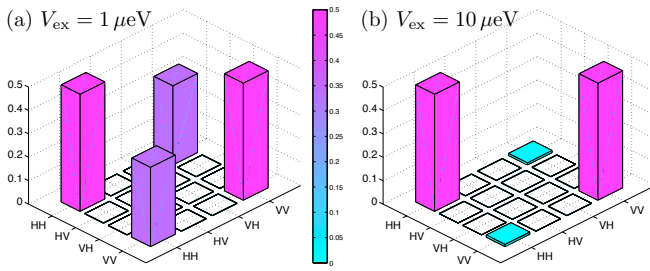


Figure 8: Quantum state tomography for (a) $V_{\text{ex}} = 1 \mu\text{eV}$ and (b) $V_{\text{ex}} = 10 \mu\text{eV}$.

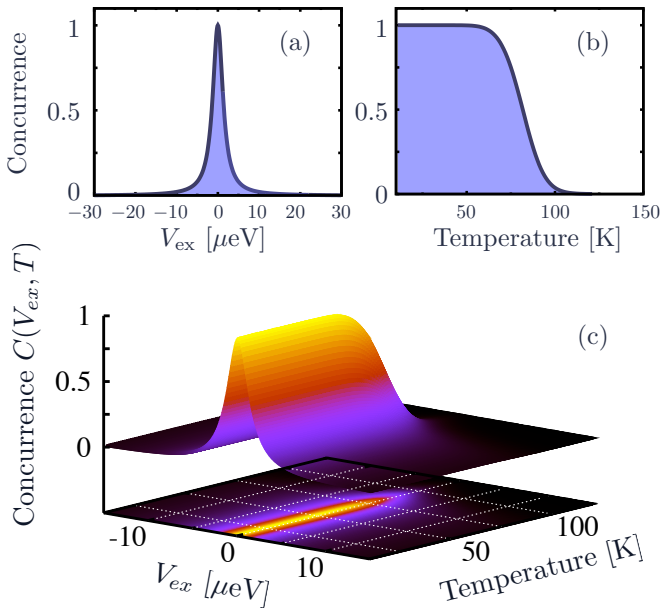


Figure 9: Plot of the concurrence. (a) displays C at 0 K as a function of V_{ex} only. (b) illustrates the influence of the temperature due to phonon-induced WL influence at $V_{\text{ex}} = 0 \mu\text{eV}$. Both temperature and V_{ex} dependence are shown in (c).

work – a temperature dependent study of entanglement. First, Fig. 9(a) shows how the entanglement is lost with increasing FFS as a continuous function of V_{ex} . Here, the FWHM is determined by the values of the Coulomb parameters. When temperature effects of the WL states are taken into account, the concurrence can be spoiled even in the ideal situation of degenerate exciton states, see Fig. 9(b). For low temperatures C will remain unaffected by the WL-induced dephasing Γ , since the scattering times are well above 1 ns, cp. Fig. 4. Starting at approximately 80 K the WL starts to affect C as Γ reaches 1 ns^{-1} , which corresponds to an energy of $0.7 \mu\text{eV}$ close to the optical coupling strength of $M = 1 \mu\text{eV}$. The entanglement decreases for zero V_{ex} until it is entirely lost for temperatures beyond 100 K. For a higher FFS with $V_{\text{ex}} \neq 0$, Fig. 9(c) shows, that the degree of entanglement is lost slightly earlier around 80 K.

Finally, to pick up on the topic of temporal dynamics

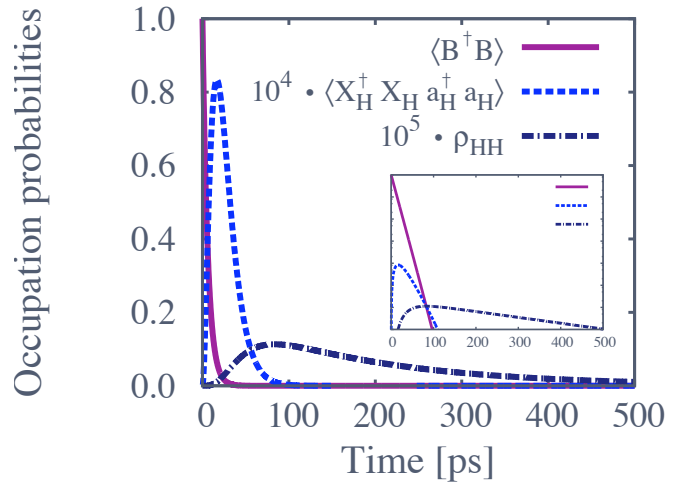


Figure 10: Dynamics of the cascade biexciton \rightarrow exciton-and-one-photon \rightarrow ground-state-and-two-photons. Results for vanishing $V_{\text{ex}} = 0 \mu\text{eV}$ at $T = 0 \text{ K}$. $\langle \hat{X}_H^\dagger \hat{X}_H \hat{a}_H^\dagger \hat{a}_H \rangle$ and ρ_{HH} are enlarged by a factor of 10^4 and 10^5 , respectively. The inset shows the dynamics on a logarithmic scale.

of the cascade already addressed in Sec. III B let us consider a direct, single path leading to no entanglement. Therefore, we will follow the blue HH (left) path in Fig. 5. The biexciton density $\langle \hat{B}^\dagger \hat{B} \rangle$ decays exponentially with 4Γ giving rise to an intermediate coupled exciton-photon state $\langle \hat{X}_H^\dagger \hat{X}_H \hat{a}_H^\dagger \hat{a}_H \rangle$. Subsequently, when this state is sufficiently populated it decays under emission of the exciton-photon and a two-photon density ρ_{HH} builds up. In the given range of parameters (see table I), Fig. 10 shows that the decay cascade happens on a ps time scale. Even at low temperatures and $V_{\text{ex}} = 0 \mu\text{eV}$, due to high cavity loss κ (compared to the optical coupling strength M) both $\langle \hat{X}_H^\dagger \hat{X}_H \hat{a}_H^\dagger \hat{a}_H \rangle$ and ρ_{HH} are only weakly occupied. The inset in Fig. 10 is a logarithmic plot of the dynamics which clearly shows the different lifetimes of the involved quantities.

V. CONCLUSION

In summary, we showed that – based on a Heisenberg-equation approach – the density matrix of the photon-polarization subspace of a biexciton, all intermediate occurring states of the cascade as well as their dynamics can be microscopically calculated. The interaction of the dot states with the WL via LO-phonons was included within this approach and gave rise to a strong reduction of the concurrence for temperatures above 100 K for typical InGaAs self-assembled QDs.

The diagonal interaction of the QD states with longitudinal phonons is a major contribution to dephasing effects,^{69,70} which will ultimately influence the quality of entanglement.¹⁸

Our conclusion is, that regardless of their impact, the inherit coupling to the WL imposes another fundamental limit to high temperature generation of polarisation-entangled photons in solid state devices.

Acknowledgments

We would like to thank Stephen Hughes for helpful discussions. This work was financially supported by the Deutsche Forschungsgemeinschaft within the Sonderforschungsbereich 787 "Nanophotonik".

Appendix A: CARRIER-CARRIER INTERACTION AND EXCITON REPRESENTATION

When constructing the single-particle basis which is to be diagonalized we can employ the fact that only a fraction of all possible QD states will contribute. First, not all transitions are optically active. A transition of a conduction band electron under emission of a photon must conserve the angular momentum. The electron-photon matrix element leads to selection rules that have to be obeyed and so only electron-hole pairs with opposite spins couple. Second, and more important, the Pauli-Principle forbids two carriers to be in the same state (that is the spin state $s = |J, m_j\rangle$).

With these considerations, only four states remain to determine the system dynamics, defined by the following operators:

$$\hat{G} = \hat{h}_\downarrow \hat{h}_\uparrow \hat{h}_\uparrow^\dagger \hat{h}_\downarrow^\dagger \quad \text{Ground state operator,} \quad (\text{A1})$$

$$\hat{B} = \hat{h}_\uparrow \hat{h}_\downarrow \hat{e}_\uparrow \hat{e}_\downarrow \quad \text{Biexciton state operator,} \quad (\text{A2})$$

$$\hat{X}_+ = \hat{h}_\uparrow \hat{h}_\downarrow \hat{h}_\uparrow^\dagger \hat{e}_\downarrow \quad \text{Exciton state operator 1,} \quad (\text{A3})$$

$$\hat{X}_- = \hat{h}_\downarrow \hat{h}_\uparrow \hat{h}_\downarrow^\dagger \hat{e}_\uparrow \quad \text{Exciton state operator 2.} \quad (\text{A4})$$

Commuting these operators with $\hat{H}_{\text{Coul}} = \hat{H}_{\text{QD},0}^c + \hat{H}_{c-c}^c$, we note, that ground state \hat{G} and biexciton operator \hat{B} are already diagonal:

$$\left[\hat{H}_{\text{Coul}}, \hat{G} \right] = \hbar\omega_G \hat{G}, \quad \left[\hat{H}_{\text{Coul}}, \hat{B} \right] = \hbar\omega_B \hat{B}, \quad (\text{A5})$$

with $\hbar\omega_G = 0$, choosing zero as ground state energy, and $\hbar\omega_B = 4E_C + 2\hbar\Omega_0 + V_{\downarrow\downarrow}^{\text{ex}} + V_{\uparrow\uparrow}^{\text{ex}}$ with $E_C = \frac{1}{2}(V^{cc} + V^{vv} - 2V^{vc})$. Investigating the exciton operators \hat{X}_\pm , we find:

$$\left[\hat{H}_{\text{Coul}}, \hat{X}_+ \right] = (E_C + \hbar\Omega_0 + V_{\downarrow\downarrow}^{\text{ex}}) \hat{X}_+ - V_{\uparrow\downarrow}^{\text{ex}} \hat{X}_- \quad (\text{A6})$$

$$\left[\hat{H}_{\text{Coul}}, \hat{X}_- \right] = (E_C + \hbar\Omega_0 + V_{\uparrow\uparrow}^{\text{ex}}) \hat{X}_- - V_{\downarrow\uparrow}^{\text{ex}} \hat{X}_+. \quad (\text{A7})$$

The exciton operators in Eqs. (A3) and (A4) emit into circular polarized light modes (σ_+ and σ_-), if the non-diagonal element $V_{\uparrow\downarrow}^{\text{ex}}$ is zero. In a reduced C_{2v} symmetry of strained dots, the off-diagonal element $V_{\uparrow\downarrow}^{\text{ex}}$ is non-zero and leads to a superposition of the exciton states,

which are not eigenstates of \hat{H}_{Coul} .⁷¹ For convenience, via solving a diagonalization problem, new exciton operators $\hat{X}_{H/V}$ are introduced. Here, H and V refer to the linear polarization of the emitted photons in the biexciton cascade:

$$\hat{X}_H = u_1^H \hat{X}_+ + u_2^H \hat{X}_-, \quad \hat{X}_V = u_1^V \hat{X}_+ + u_2^V \hat{X}_-. \quad (\text{A8})$$

The unitary transformation coefficients are given by

$$u_1^H = -u_2^V = -(1 + \Delta_e^2)^{-\frac{1}{2}} \Delta_e, \\ u_2^H = u_1^V = (1 + \Delta_e^2)^{-\frac{1}{2}},$$

where $\Delta_e = V_{\text{ex}}(E_C + \hbar\Omega_0 + V_{\downarrow\downarrow}^{\text{ex}} - \hbar\omega_H)^{-1} = -V_{\text{ex}}(E_C + \hbar\Omega_0 + V_{\uparrow\uparrow}^{\text{ex}} - \hbar\omega_V)^{-1}$ and $V_{\text{ex}} = V_{\uparrow\downarrow}^{\text{ex}} = V_{\downarrow\uparrow}^{\text{ex}}$. Within the new excitonic basis the electron operators ($\hat{G}^{(\dagger)}$, $\hat{X}_H^{(\dagger)}$, $\hat{X}_V^{(\dagger)}$, $\hat{B}^{(\dagger)}$) are eigenvectors to $\hat{H}_{\text{QD},0}^c + \hat{H}_{\text{QD}}^c$. Their corresponding eigenvalues are $(\hbar\omega_G, \hbar\omega_H, \hbar\omega_V, \hbar\omega_B)$ with exciton energies $\hbar\omega_H$ and $\hbar\omega_V$ in the two-particle basis:

$$\hbar\omega_{H/V} = \frac{1}{2} (2E_C + 2\hbar\Omega_0 + V_{\downarrow\downarrow}^{\text{ex}} + V_{\uparrow\uparrow}^{\text{ex}} \pm \delta). \quad (\text{A9})$$

Responsible for the fine structure splitting δ , compare Fig. 1, is the exchange splitting $V_{\uparrow\downarrow}^{\text{ex}}$, which describes the repulsion and attraction forces induced by different spin-conformations of electrons and holes. In the most general case, the exciton states could differ in energy due to contributions like $V_{\uparrow\uparrow}^{\text{ex}}$ and $V_{\downarrow\downarrow}^{\text{ex}}$. Given these elements, the most general fine structure splitting can now be expressed

quantitatively as $\delta := \sqrt{(V_{\uparrow\uparrow}^{\text{ex}} - V_{\downarrow\downarrow}^{\text{ex}})^2 + 4|V_{\uparrow\downarrow}^{\text{ex}}|^2}$. However, it is reasonable to assume that in semiconductor QD no spin-preferences exist, thus $V_{\uparrow\uparrow}^{\text{ex}} - V_{\downarrow\downarrow}^{\text{ex}} = 0$, which leads to

$$\delta = 2 |V_{\uparrow\downarrow}^{\text{ex}}|. \quad (\text{A10})$$

In our case of no spin-preferences, where $(V_{\downarrow\downarrow}^{\text{ex}} - V_{\uparrow\uparrow}^{\text{ex}}) = 0$, it follows that $\Delta_e = -1$, $u_1^H = u_2^H = u_1^V = -u_2^V = \frac{1}{\sqrt{2}}$, and thus explicitly

$$\hat{X}_H = \frac{1}{\sqrt{2}} (\hat{X}_+ + \hat{X}_-), \quad \hat{X}_V = \frac{1}{\sqrt{2}} (\hat{X}_+ - \hat{X}_-). \quad (\text{A11})$$

Appendix B: QD ELECTRON-PHOTON INTERACTION

Starting with Eq. (17), we now switch to the new exciton operators $\hat{X}_{H/V}$ by inserting the unity relation of the electron-hole picture into Eq. (17). After normal ordering and using the two-electron assumption, the electron-light interaction can be written as:⁶²

$$\hat{H}_{\text{QD}}^{\text{c-pt}} = \hbar M \sum_i \left(\hat{G}^\dagger \hat{X}_+ + \hat{X}_- \hat{B} \right) \hat{a}_{i\sigma_+}^\dagger \quad (\text{B1}) \\ + \hbar M \sum_i \left(\hat{G}^\dagger \hat{X}_- + \hat{X}_+ \hat{B} \right) \hat{a}_{i\sigma_-}^\dagger + \text{h.a.}$$

The electron-light interaction Hamiltonian $\hat{H}_{\text{QD}}^{\text{c-pt}}$ is transformed, when the exciton operators are replaced with:

$$\hat{X}_+ = \frac{1}{\sqrt{2}} (\hat{X}_H + \hat{X}_V), \quad \hat{X}_- = \frac{1}{\sqrt{2}} (\hat{X}_H - \hat{X}_V). \quad (\text{B2})$$

It is convenient to define new photon operators:

$$\begin{aligned} \hat{a}_{iH}^\dagger &= \frac{1}{\sqrt{2}} (\hat{a}_{i\sigma_+}^\dagger + \hat{a}_{i\sigma_-}^\dagger), \\ \hat{a}_{iV}^\dagger &= \frac{1}{\sqrt{2}} (\hat{a}_{i\sigma_+}^\dagger - \hat{a}_{i\sigma_-}^\dagger). \end{aligned} \quad (\text{B3})$$

The Hamiltonian now takes the form:

$$\begin{aligned} \hat{H}_{\text{QD}}^{\text{c-pt}} &= \hbar M \sum_i \left(\hat{G}^\dagger \hat{X}_H \hat{a}_{iH}^\dagger + \hat{G}^\dagger \hat{X}_V \hat{a}_{iV}^\dagger \right) \\ &+ \hbar M \sum_i \left(\hat{X}_H^\dagger \hat{B} \hat{a}_{iH}^\dagger - \hat{X}_V^\dagger \hat{B} \hat{a}_{iV}^\dagger \right) + \text{h.a.} \end{aligned} \quad (\text{B4})$$

Appendix C: EQUATIONS OF MOTION

The temporal evolution of the driving terms in Eq. (20) is given by

$$\begin{aligned} \partial_t \langle \hat{G}^\dagger \hat{X}_H \hat{a}_V^\dagger \hat{a}_V^\dagger \hat{a}_H \rangle &= \\ i(-\omega_H + 2\omega_V^{\text{cav}} - \omega_H^{\text{cav}} + i\Gamma + 3i\kappa) \langle \hat{G}^\dagger \hat{X}_H \hat{a}_V^\dagger \hat{a}_V^\dagger \hat{a}_H \rangle \\ - 2iM \langle \hat{X}_V^\dagger \hat{X}_H \hat{a}_V^\dagger \hat{a}_H \rangle + iM \langle \hat{G}^\dagger \hat{B} \hat{a}_V^\dagger \hat{a}_V^\dagger \rangle \end{aligned} \quad (\text{C1})$$

and

$$\begin{aligned} \partial_t \langle \hat{X}_V^\dagger \hat{G} \hat{a}_V^\dagger \hat{a}_H \hat{a}_H \rangle &= \\ i(\omega_V + \omega_V^{\text{cav}} - 2\omega_H^{\text{cav}} + i\Gamma + 3i\kappa) \langle \hat{X}_V^\dagger \hat{G} \hat{a}_V^\dagger \hat{a}_H \hat{a}_H \rangle \\ + 2iM \langle \hat{X}_V^\dagger \hat{X}_H \hat{a}_V^\dagger \hat{a}_H \rangle + iM \langle \hat{B}^\dagger \hat{G} \hat{a}_H \hat{a}_H \rangle. \end{aligned} \quad (\text{C2})$$

The driving terms of the two-photon density matrix in turn couple to combined exciton- and photon coherences $\hat{X}_V^\dagger \hat{X}_H \hat{a}_V^\dagger \hat{a}_H$ and to the direct decay channel from $|B\rangle$ to $|G\rangle$ emitting two photons with the same polarization $\hat{G}^\dagger \hat{B} \hat{a}_V^\dagger \hat{a}_V^\dagger$, see orange box in Fig. 5. Crucial for entangling the two decay paths is the exciton coherence, assisted by a photon coherence, see red box in Fig. 5:

$$\begin{aligned} \partial_t \langle \hat{X}_V^\dagger \hat{X}_H \hat{a}_V^\dagger \hat{a}_H \rangle &= \\ i(\omega_V - \omega_H + \omega_V^{\text{cav}} - \omega_H^{\text{cav}} + 2i\Gamma + 2i\kappa) \langle \hat{X}_V^\dagger \hat{X}_H \hat{a}_V^\dagger \hat{a}_H \rangle \\ - iM \langle \hat{G}^\dagger \hat{X}_H \hat{a}_V^\dagger \hat{a}_V^\dagger \hat{a}_H \rangle + iM \langle \hat{B}^\dagger \hat{X}_H \hat{a}_H \rangle \\ + iM \langle \hat{X}_V^\dagger \hat{G} \hat{a}_V^\dagger \hat{a}_H \hat{a}_H \rangle + iM \langle \hat{X}_V^\dagger \hat{B} \hat{a}_V^\dagger \rangle. \end{aligned} \quad (\text{C3})$$

In this equation, the two paths interfere. The influence in the two-particle correlation $\langle \hat{X}_V^\dagger \hat{X}_H \hat{a}_V^\dagger \hat{a}_H \rangle$ increases the

degree of entanglement as this term couples back to the driving terms of ρ_{VH} , Eq. (C1) and (C2). Here again the resonance condition of the frequencies is essential ($\omega_V - \omega_H = \omega_V^{\text{cav}} - \omega_H^{\text{cav}} = \delta$): A high detuning δ will diminish the contribution of Eq. (C3) to the cascade and both paths cannot interfere.

The other characteristic and important quantity in the two-electron biexciton-cascade situation (cp. with two coupled QDs⁶²) are the two-photon polarizations

$$\begin{aligned} \partial_t \langle \hat{G}^\dagger \hat{B} \hat{a}_V^\dagger \hat{a}_V^\dagger \rangle &= \\ i(-\omega_B + 2\omega_V^{\text{cav}} + 2i\Gamma + 2i\kappa) \langle \hat{G}^\dagger \hat{B} \hat{a}_V^\dagger \hat{a}_V^\dagger \rangle \\ + iM \langle \hat{G}^\dagger \hat{X}_H \hat{a}_V^\dagger \hat{a}_V^\dagger \hat{a}_H \rangle - iM \langle \hat{G}^\dagger \hat{X}_V \hat{a}_V^\dagger \hat{a}_V^\dagger \hat{a}_V \rangle \\ - 2iM \langle \hat{X}_V^\dagger \hat{B} \hat{a}_V^\dagger \rangle \end{aligned} \quad (\text{C4})$$

and

$$\begin{aligned} \partial_t \langle \hat{B}^\dagger \hat{G} \hat{a}_H \hat{a}_H \rangle &= \\ i(\omega_B - 2\omega_H^{\text{cav}} + 2i\Gamma + 2i\kappa) \langle \hat{B}^\dagger \hat{G} \hat{a}_H \hat{a}_H \rangle \\ - iM \langle \hat{X}_H^\dagger \hat{G} \hat{a}_H^\dagger \hat{a}_H \hat{a}_H \rangle + iM \langle \hat{X}_V^\dagger \hat{G} \hat{a}_V^\dagger \hat{a}_H \hat{a}_H \rangle \end{aligned} \quad (\text{C5})$$

$$\begin{aligned} + 2iM \langle \hat{B}^\dagger \hat{X}_H \hat{a}_H \rangle. \end{aligned} \quad (\text{C6})$$

Each path in the cascade has one biexciton-to-ground state transition like $\hat{G}^\dagger \hat{B} \hat{a}_V^\dagger \hat{a}_V^\dagger$. Its dynamics couples the biexciton-to-exciton transition $\hat{X}_V^\dagger \hat{B} \hat{a}_V^\dagger$ with both exciton-to-ground state transitions $\hat{G}^\dagger \hat{X}_i$. Remarkably, the origin of the entanglement is directly visible, since a quantity of a different path enters in Eq. (C4): $\langle \hat{G}^\dagger \hat{X}_H \hat{a}_V^\dagger \hat{a}_V^\dagger \hat{a}_H \rangle$. Here again, the two paths interfere. For maximum entanglement the contributions of the different paths $\hat{G}^\dagger \hat{X}_H$ and $\hat{G}^\dagger \hat{X}_V$ to the expectation values should be equally weighted. The photon-assisted biexciton-to-exciton transition enters in the two-photon polarization and drives this quantity via the biexciton decay:

$$\begin{aligned} \partial_t \langle \hat{B}^\dagger \hat{X}_H \hat{a}_H \rangle &= \\ i(\omega_B - \omega_H - \omega_H^{\text{cav}} + 3i\Gamma + i\kappa) \langle \hat{B}^\dagger \hat{X}_H \hat{a}_H \rangle \\ - iM \langle \hat{X}_H^\dagger \hat{X}_H \hat{a}_H^\dagger \hat{a}_H \rangle + iM \langle \hat{X}_V^\dagger \hat{X}_H \hat{a}_V^\dagger \hat{a}_H \rangle \\ + iM \langle \hat{B}^\dagger \hat{B} \rangle + iM \langle \hat{B}^\dagger \hat{G} \hat{a}_H \hat{a}_H \rangle, \end{aligned} \quad (\text{C7})$$

$$\begin{aligned} \partial_t \langle \hat{X}_V^\dagger \hat{B} \hat{a}_V^\dagger \rangle &= \\ i(-\omega_B + \omega_V + \omega_V^{\text{cav}} + 3i\Gamma + i\kappa) \langle \hat{X}_V^\dagger \hat{B} \hat{a}_V^\dagger \rangle \\ - iM \langle \hat{G}^\dagger \hat{B} \hat{a}_V^\dagger \hat{a}_V^\dagger \rangle + iM \langle \hat{B}^\dagger \hat{B} \rangle \\ + iM \langle \hat{X}_V^\dagger \hat{X}_H \hat{a}_V^\dagger \hat{a}_H \rangle - iM \langle \hat{X}_V^\dagger \hat{X}_V \hat{a}_V^\dagger \hat{a}_V \rangle. \end{aligned} \quad (\text{C8})$$

The occurring biexciton as well as the intermediate exciton-photon densities are driven by the biexciton-exciton transition $\langle \hat{X}_i^\dagger \hat{B} \hat{a}_i^\dagger \rangle$:

$$\begin{aligned} \partial_t \langle \hat{X}_H^\dagger \hat{X}_H \hat{a}_H^\dagger \hat{a}_H \rangle = & \\ - (2\Gamma + 2\kappa) \langle \hat{X}_H^\dagger \hat{X}_H \hat{a}_H^\dagger \hat{a}_H \rangle & \quad (C9) \\ - 2 \operatorname{Im} \left(M \langle \hat{X}_H^\dagger \hat{B} \hat{a}_H^\dagger \rangle + M \langle \hat{X}_H^\dagger \hat{G} \hat{a}_H^\dagger \hat{a}_H \hat{a}_H \rangle \right), & \end{aligned}$$

$$\begin{aligned} \partial_t \langle \hat{X}_V^\dagger \hat{X}_V \hat{a}_V^\dagger \hat{a}_V \rangle = & \\ - (2\Gamma + 2\kappa) \langle \hat{X}_V^\dagger \hat{X}_V \hat{a}_V^\dagger \hat{a}_V \rangle & \quad (C10) \\ + 2 \operatorname{Im} \left(M \langle \hat{X}_V^\dagger \hat{B} \hat{a}_V^\dagger \rangle - M \langle \hat{X}_V^\dagger \hat{G} \hat{a}_V^\dagger \hat{a}_V \hat{a}_V \rangle \right). & \end{aligned}$$

From the perspective of the cascade our course of action so far put the cart before the horse since the actual dynamics start with a loaded biexciton density $\langle \hat{B}^\dagger \hat{B} \rangle$. In the visualization of the complex interplay, Fig. 5, we followed a bottom-to-top trail through the cascade, starting with the concurrence determining ρ_{VH} . The biexciton $\langle \hat{B}^\dagger \hat{B} \rangle$ as the top element of the scheme decays via the H or the V intermediate exciton-to-ground-state path

$$\begin{aligned} \partial_t \langle \hat{B}^\dagger \hat{B} \rangle = -4\Gamma \langle \hat{B}^\dagger \hat{B} \rangle & \quad (C11) \\ + 2 \operatorname{Im} \left(M \langle \hat{X}_H^\dagger \hat{B} \hat{a}_H^\dagger \rangle - M \langle \hat{X}_V^\dagger \hat{B} \hat{a}_V^\dagger \rangle \right). & \end{aligned}$$

To complete the set of equation, two higher-order photon-assisted exciton-to-ground state transitions of the direct and thus not entangled path are necessary:

$$\begin{aligned} \partial_t \langle \hat{G}^\dagger \hat{X}_H \hat{a}_H^\dagger \hat{a}_H^\dagger \hat{a}_H \rangle = & \\ i(-\omega_H + \omega_H^{\text{cav}} + i\Gamma + 3i\kappa) \langle \hat{G}^\dagger \hat{X}_H \hat{a}_H^\dagger \hat{a}_H^\dagger \hat{a}_H \rangle & \quad (C12) \\ - 2iM \langle \hat{X}_H^\dagger \hat{X}_H \hat{a}_H^\dagger \hat{a}_H \rangle + iM \langle \hat{G}^\dagger \hat{B} \hat{a}_H^\dagger \hat{a}_H^\dagger \rangle, & \end{aligned}$$

$$\begin{aligned} \partial_t \langle \hat{G}^\dagger \hat{X}_V \hat{a}_V^\dagger \hat{a}_V^\dagger \hat{a}_V \rangle = & \\ i(-\omega_V + \omega_V^{\text{cav}} + i\Gamma + 3i\kappa) \langle \hat{G}^\dagger \hat{X}_V \hat{a}_V^\dagger \hat{a}_V^\dagger \hat{a}_V \rangle & \quad (C13) \\ - 2iM \langle \hat{X}_V^\dagger \hat{X}_V \hat{a}_V^\dagger \hat{a}_V \rangle - iM \langle \hat{G}^\dagger \hat{B} \hat{a}_V^\dagger \hat{a}_V^\dagger \rangle. & \end{aligned}$$

With these polarization Eq. (C12-C13), the diagonal elements $i = H, V$ of the density matrix of the polarization subspace are given, too:

$$\begin{aligned} \partial_t \langle \hat{a}_i^\dagger \hat{a}_i^\dagger \hat{a}_i \hat{a}_i \rangle = & \\ -4\kappa \langle \hat{a}_i^\dagger \hat{a}_i^\dagger \hat{a}_i \hat{a}_i \rangle - 4 \operatorname{Im} \left(M \langle \hat{G}^\dagger \hat{X}_i \hat{a}_i^\dagger \hat{a}_i^\dagger \hat{a}_i \rangle \right). & \quad (C14) \end{aligned}$$

* E-mail at: alex@itp.physik.tu-berlin.de

- ¹ M. A. Nielsen and I. L. Chuang, *Quantum Computation and Quantum Information* (Cambridge University Press, Cambridge, 2000).
- ² T. B. Pittman, B. C. Jacobs, and J. D. Franson, Phys. Rev. A **66**, 042303 (2002).
- ³ D. Stucki, N. Gisin, O. Guinnard, G. Ribordy, and H. Zbinden, New J. Phys. **4**, 41 (2002), URL <http://stacks.iop.org/1367-2630/4/41>.
- ⁴ N. Gisin, G. Ribordy, W. Tittel, and H. Zbinden, Rev. Mod. Phys. **74**, 145 (2002).
- ⁵ A. Poppe, A. Fedrizzi, R. Ursin, H. Bohm, T. Lorunser, O. Maurhardt, M. Peev, M. Suda, C. Kurtsiefer, H. Weinfurter, et al., Opt. Express **12**, 3865 (2004).
- ⁶ D. Bouwmeester, J. Pan, K. Mattle, M. Eibl, H. Weinfurter, and A. Zeilinger, Nature **390**, 575 (1997).
- ⁷ C. H. Bennett, G. Brassard, C. Crépeau, R. Jozsa, A. Peres, and W. K. Wootters, Phys. Rev. Lett. **70**, 1895 (1993).
- ⁸ S. Scheel, W. J. Munro, J. Eisert, K. Nemoto, and P. Kok, Phys. Rev. A. **73**, 034301 (2006), URL <http://link.aps.org/abstract/PRA/v73/e034301>.
- ⁹ J. Brendel, N. Gisin, W. Tittel, and H. Zbinden, Phys. Rev. Lett. **82**, 2594 (1999).
- ¹⁰ K. Edamatsu, G. Oohata, R. Shimizu, and T. Itoh, Na-

ture **431**, 167 (2004), URL <http://dx.doi.org/10.1038/nature02838>.

- ¹¹ S. Fasel, O. Alibart, S. Tanzilli, P. Baldi, A. Beveratos, N. Gisin, and H. Zbinden, New J. Phys. **6**, 163 (2004), URL <http://stacks.iop.org/1367-2630/6/163>.
- ¹² Z. Y. Ou and L. Mandel, Phys. Rev. Lett. **61**, 50 (1988).
- ¹³ Y. H. Shih and C. O. Alley, Phys. Rev. Lett. **61**, 2921 (1988).
- ¹⁴ O. Benson, C. Santori, M. Pelton, and Y. Yamamoto, Phys. Rev. Lett. **84**, 2513 (2000).
- ¹⁵ D. C. Burnham and D. L. Weinberg, Phys. Rev. Lett. **25**, 84 (1970).
- ¹⁶ M. Bayer, T. L. Reinecke, F. Weidner, A. Larionov, A. McDonald, and A. Forchel, Phys. Rev. Lett. **86**, 3168 (2001).
- ¹⁷ V. M. Axt, T. Kuhn, A. Vagov, and F. M. Peeters, Phys. Rev. B **72**, 125309 (2005), URL <http://link.aps.org/abstract/PRB/v72/e125309>.
- ¹⁸ U. Hohenester, G. Pfanner, and M. Seliger, Phys. Rev. Lett. **99**, 047402 (2007).
- ¹⁹ D. Bimberg, M. Grundmann, and N. N. Ledentsov, *Quantum Dot Heterostructures* (John Wiley & Sons, Chichester, 1999).
- ²⁰ T. Inoshita and H. Sakaki, Phys. Rev. B **46**, 7260 (1992).
- ²¹ J. Bell, Physics **1**, 195 (1964).
- ²² A. Peres, Phys. Rev. Lett. **77**, 1413 (1996).

- ²³ O. Stier, M. Grundmann, and D. Bimberg, *Phys. Rev. B* **59**, 5688 (1999).
- ²⁴ P. Y. Yu and M. Cardona, *Fundamentals of Semiconductors* (Springer, Berlin, 2005).
- ²⁵ A. L. Efros, M. Rosen, M. Kuno, M. Nirmal, D. J. Norris, and M. Bawendi, *Phys. Rev. B* **54**, 4843 (1996).
- ²⁶ C. Weisbuch and B. Winter, *Quantum Semiconductor Structures* (Academic Press, San Diego, 1991).
- ²⁷ G. D. Scholes, *J. Chem. Phys.* **121**, 10104 (2004), URL <http://link.aip.org/link/?JCP/121/10104/1>.
- ²⁸ Z. Yuan, B. E. Kardynal, R. M. Stevenson, A. J. Shields., C. J. Lob, K. Cooper, N. S. Beattie, D. A. Ritchie, and M. Pepper, *Science* **295**, 102 (2002), URL <http://www.sciencemag.org/cgi/content/abstract/295/5552/102>.
- ²⁹ A. Lochmann, E. Stock, J. Töfflinger, W. Unrau, A. Toropov, A. Bakarov, V. Haisler, and D. Bimberg, *Electron. Lett.* **45**, 566 (2009), URL <http://link.aip.org/link/?ELL/45/566/1>.
- ³⁰ K. Edamatsu, *Jpn. J. Appl. Phys.* **46**, 7175 (2007), URL <http://jjap.ipap.jp/link?JJAP/46/7175/>.
- ³¹ R. Seguin, A. Schliwa, T. D. Germann, S. Rodt, K. Pötschke, A. Strittmatter, U. W. Pohl, D. Bimberg, M. Winkelnkemper, T. Hammerschmidt, et al., *Appl. Phys. Lett.* **89**, 263109 (2006), URL <http://link.aip.org/link/?APL/89/263109/1>.
- ³² K. Hennessy, C. Högerle, E. Hu, A. Badolato, and A. Imamoglu, *Appl. Phys. Lett.* **89**, 041118 (2006), URL <http://link.aip.org/link/?APL/89/041118/1>.
- ³³ M. E. Reimer, M. Korkusiński, D. Dalacu, J. Lefebvre, J. Lapointe, P. J. Poole, G. C. Aers, W. R. McKinnon, P. Hawrylak, and R. L. Williams, *Phys. Rev. B* **78**, 195301 (2008), URL <http://link.aps.org/abstract/PRB/v78/e195301>.
- ³⁴ M. Korkusiński, M. E. Reimer, R. L. Williams, and P. Hawrylak, *Phys. Rev. B* **79**, 035309 (2009), URL <http://link.aps.org/abstract/PRB/v79/e035309>.
- ³⁵ R. M. Stevenson, R. J. Young, P. See, D. G. Gevaux, K. Cooper, P. Atkinson, I. Farrer, D. A. Ritchie, and A. J. Shields, *Phys. Rev. B* **73**, 033306 (2006), URL <http://link.aps.org/abstract/PRB/v73/e033306>.
- ³⁶ R. M. Stevenson, R. Young, P. Atkinson, K. Cooper, D. Ritchie, and A. Shields, *Nature* **439**, 179 (2006).
- ³⁷ D. F. V. James, P. G. Kwiat, W. J. Munro, and A. G. White, *Phys. Rev. A* **64**, 052312 (2001).
- ³⁸ L. Mandel and E. Wolf, *Optical coherence and quantum optics* (Cambridge University Press, Cambridge, 1995).
- ³⁹ F. Troiani, J. I. Perea, and C. Tejedor, *Phys. Rev. B* **74**, 235310 (2006).
- ⁴⁰ M. Benyoucef, S. M. Ulrich, P. Michler, J. Wiersig, F. Jahnke, and A. Forchel, *New J. Phys.* **6**, 91 (2004), URL <http://stacks.iop.org/1367-2630/6/91>.
- ⁴¹ W. K. Wootters, *Phys. Rev. Lett.* **80**, 2245 (1998).
- ⁴² V. Coffman, J. Kundu, and W. K. Wootters, *Phys. Rev. A* **61**, 052306 (2000).
- ⁴³ C. H. Bennett, D. P. DiVincenzo, J. A. Smolin, and W. K. Wootters, *Phys. Rev. A* **54**, 3824 (1996).
- ⁴⁴ A. G. White, D. F. V. James, W. J. Munro, and P. G. Kwiat, *Phys. Rev. A* **65**, 012301 (2001).
- ⁴⁵ M. Vachon, S. Raymond, A. Babinski, J. Lapointe, Z. Wasilewski, and M. Potemski, *Phys. Rev. B* **79**, 165427 (2009), URL <http://link.aps.org/abstract/PRB/v79/e165427>.
- ⁴⁶ E. A. Muljarov and R. Zimmermann, *Phys. Rev. Lett.* **98**, 187401 (2007), URL <http://link.aps.org/abstract/PRL/v98/e187401>.
- ⁴⁷ E. A. Muljarov and R. Zimmermann, *Phys. Status Solidi B* **245**, 1106 (2008).
- ⁴⁸ J. Seebeck, T. R. Nielsen, P. Gartner, and F. Jahnke, *Phys. Rev. B* **71**, 125327 (2005), URL <http://link.aps.org/abstract/PRB/v71/e125327>.
- ⁴⁹ I. Magnúsdóttir, A. V. Uskov, S. Bischoff, B. Tromborg, and J. Mørk, *J. Appl. Phys.* **92**, 5982 (2002).
- ⁵⁰ P. Machnikowski, *Phys. Rev. B* **78**, 195320 (2008), URL <http://link.aps.org/abstract/PRB/v78/e195320>.
- ⁵¹ B. Krummheuer, V. M. Axt, T. Kuhn, I. D'Amico, and F. Rossi, *Phys. Rev. B* **71**, 235329 (2005), URL <http://link.aps.org/abstract/PRB/v71/e235329>.
- ⁵² M. Lorke, T. R. Nielsen, J. Seebeck, P. Gartner, and F. Jahnke, *Phys. Rev. B* **73**, 085324 (pages 10) (2006), URL <http://link.aps.org/abstract/PRB/v73/e085324>.
- ⁵³ F. H. M. Faisal, *Theory of Multiphoton Processes* (Plenum Press, London, 1987).
- ⁵⁴ G. D. Mahan, *Many-Particle Physics* (Plenum Press, New York, 1990).
- ⁵⁵ M.-R. Dachner, E. Malić, M. Richter, A. Carmele, J. Kabuß, A. Wilms, J.-E. Kim, G. Hartmann, J. Wolters, U. Bandelow, et al., *Phys. Status Solidi B* (submitted) (2009).
- ⁵⁶ J. Wolters, M.-R. Dachner, E. Malić, M. Richter, U. Woggon, and A. Knorr, *Phys. Rev. B* (submitted) (2009).
- ⁵⁷ I. Waldmueller, W. W. Chow, E. W. Young, and M. C. Wanke, *IEEE J. Quantum Electron.* **42**, 292 (2006).
- ⁵⁸ M.-R. Dachner, J. Wolters, A. Knorr, and M. Richter, in *Conference on Lasers and Electro-Optics/International Quantum Electronics Conference* (Optical Society of America, 2009), p. JWA119, URL <http://www.opticsinfobase.org/abstract.cfm?URI=URI=CLEO-2009-JWA119>.
- ⁵⁹ T. Takagahara, *Phys. Rev. B* **62**, 16840 (2000).
- ⁶⁰ T. Takagahara, *Phys. Rev. B* **47**, 4569 (1993).
- ⁶¹ M. Richter, K. J. Ahn, A. Knorr, A. Schliwa, D. Bimberg, M. E.-A. Madjet, and T. Renger, *Phys. Status Solidi B* **243**, 2302 (2006).
- ⁶² A. Carmele, A. Knorr, and M. Richter, *Phys. Rev. B* **79**, 035316 (2009).
- ⁶³ W. Langbein, P. Borri, U. Woggon, V. Stavarache, D. Reuter, and A. D. Wieck, *Phys. Rev. B* **69**, 161301(R) (2004).
- ⁶⁴ U. Rössler, ed., *Group IV Elements, IV-IV and III-V Compounds*, vol. III/41b of *Landolt-Börnstein - Group III Condensed Matter* (Springer, 2002).
- ⁶⁵ K. J. Ahn, J. Förstner, and A. Knorr, *Phys. Rev. B* **71**, 153309 (2005), URL <http://link.aps.org/abstract/PRB/v71/e153309>.
- ⁶⁶ M. Richter, A. Carmele, A. Sitek, and A. Knorr, *Phys. Rev. Lett.* **103**, 087407 (2009), URL <http://link.aps.org/abstract/PRL/v103/e087407>.
- ⁶⁷ H. Carmichael, *Statistical Methods in Quantum Optics 1 - Master Equation and Fokker-Planck Equations* (Springer, Berlin Heidelberg New York, 1999).
- ⁶⁸ M. O. Scully and M. S. Zubairy, *Quantum Optics* (Cambridge University Press, Cambridge, 1997).
- ⁶⁹ P. Borri, W. Langbein, S. Schneider, U. Woggon, R. L. Sellin, D. Ouyang, and D. Bimberg, *Phys. Rev. Lett.* **87**, 157401 (2001).
- ⁷⁰ F. Milde, A. Knorr, and S. Hughes, *Phys. Rev. B* **78**, 035330 (2008).
- ⁷¹ J. Danckwerts, K. J. Ahn, J. Förstner, and A. Knorr, *Phys.*

Rev. B **73**, 165318 (2006).